

Object Preserving Siamese Network for Single Object Tracking on Point Clouds

Kaijie Zhao, Haitao Zhao, Zhongze Wang, Jingchao Peng, Zhengwei Hu
East China University of Science and Technology
No.130, Meilong Rd, Shanghai

Abstract

Obviously, the object is the key factor of the 3D single object tracking (SOT) task. However, previous Siamese-based trackers overlook the negative effects brought by randomly dropped object points during backbone sampling, which hinder trackers to predict accurate bounding boxes (BBoxes). Exploring an approach that seeks to maximize the preservation of object points and their object-aware features is of particular significance. Motivated by this, we propose an Object Preserving Siamese Network (OP-SNet), which can significantly maintain object integrity and boost tracking performance. Firstly, the **object highlighting module** enhances the object-aware features and extracts discriminative features from template and search area. Then, the **object-preserved sampling** selects object candidates to obtain object-preserved search area seeds and drop the background points that contribute less to tracking. Finally, the **object localization network** precisely locates 3D BBoxes based on the object-preserved search area seeds. Extensive experiments demonstrate our method outperforms the state-of-the-art performance ($\sim 9.4\%$ and $\sim 2.5\%$ success gain on KITTI and Waymo Open Dataset respectively).

1. Introduction

Single object tracking (SOT) has become a significant issue of computer vision, which contributes widely to various fields, such as autonomous driving [15, 18], security surveillance [26, 30] and robotics [2, 11], etc. With the fast development of 3D sensors, such as LiDAR, 3D data reflecting real-world coordinates and object sizes can be captured. Therefore, 3D computer vision tasks attract more and more attention in recent years [10, 16]. 3D single object tracking is also an essential part of 3D computer vision, which aims to improve autonomous cars' safety via predicting accurate object trajectories. At present, many 2D single object tracking algorithms have been proposed and proved their efficiency, but they cannot directly handle 3D data since 3D point clouds are of sparsity and non-uniformity [23].

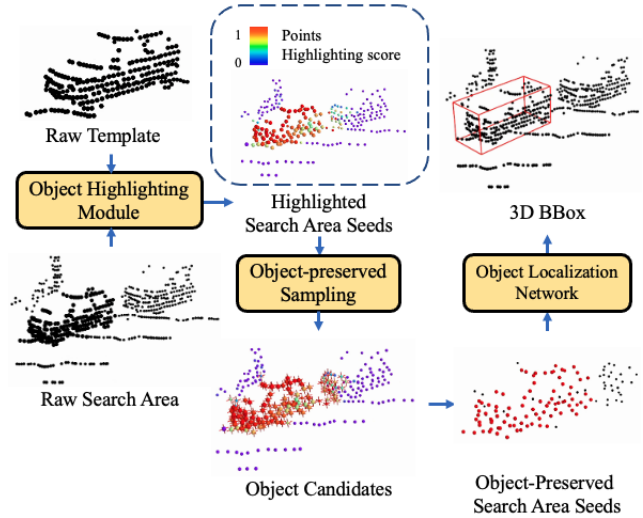


Figure 1. Exemplified illustration to show how our OPSNet works, from the object highlighting module to the object-preserved sampling and localization module.

Mainstream 3D SOT approaches are based on the Siamese network [7–9, 23, 32, 34] that consists of two weight-shared backbone branches to respectively handle template and search area. Most of the Siamese-based approaches use PointNet++ [22] as the backbone which hierarchically samples points and aggregates local features from raw point clouds. STNet [9] firstly adopts Transformer as the backbone for encoding all the points of template and search area. Considering that the tracking tasks require to be conducted in real-time and tracking speed is also a significant evaluation indicator, the PointNet++ is of higher efficiency and less computational burden [22].

Since PointNet++ applies furthest points sampling (FPS) or random sampling, all the approaches based on PointNet++ suffer from the negative effects brought by randomly dropped object points. To overcome this issue, PTTR [34] samples the search area points that are most similar to template points in the embedding space for object preservation. However, once PTTR regresses an inaccurate 3D BBox as a template during inference, search area sampling will be

simultaneously misled. Exploring a robust approach that seeks to maximize the preservation of object points and their object-aware features for tracking is of particular significance. We propose our novel OPSNet for object highlighting, object preservation, and accurate object localization.

We exemplify how our OPSNet works in Fig. 1. The object highlighting module consists of three main parts: 1) The backbone first obtains template and search area seeds (each seed is represented as $[x; f] \in \mathbb{R}^{3+d_1}$, where x denotes the 3D coordinates of the seed and f is the seed features vector), then feature-targeted transformation converts the search area seeds into two feature-targeted seed subsets, 2) adaptive cross-correlation utilizes two branches to respectively handle two feature-targeted subsets, one branch highlights object-aware features from the consistency between the subset and the template; the other branch extracts discriminative features from the discrepancy between the subset and the template, 3) object augmentation concatenates the two subsets and further obtains highlighted search area seeds with the cross attention mechanism. Each seed is appended with a highlighting score predicted by MLP, the score is supervised by smooth point-wise one-hot label and Focal Loss [14].

Obtained the highlighted search area seeds and the highlighting scores, the object-preserved sampling selects the seeds with top k highlighting scores as object candidates, Then, each object candidate clusters the neighbor seeds to aggregate local features, and we can obtain the object-preserved search area seeds. Object integrity and object-aware features can be effectively preserved and the background points that cause redundancy have been dropped simultaneously. Finally, the object localization network performs effective BBoxes prediction based on the object-preserved search area seeds without generating multiple proposals.

Experimental results (average success gain of $\sim 9.4\%$ and $\sim 2.5\%$ over the SOTA method on KITTI [6] and Waymo Open Dataset [25]) demonstrate that OPSNet achieves high-performance tracking, handles sparse point clouds effectively, and performs robust tracking on long sequences.

The contributions of this paper are as follows:

- Object highlighting module adaptively extracts not only highlighted object-aware features but also discriminative features from template and search area.
- Object-preserved sampling significantly maintains the object integrity and reduces the misleading background points and redundancy.
- Object localization network performs more effective BBoxes prediction than other voting-based regression approaches without generating multiple proposals.

2. Related Work

Deep learning on point clouds. Since Qi *et al.* [21] proposed their inspirational paradigm PointNet, 3D deep learning on point clouds has stimulated the interest of researchers. 3D deep learning on point clouds methods mainly consist of point-based [4, 22, 23, 31], voxel-based [13, 35, 36], graph-based [20, 27]. We choose the point-based method since the point-based method learns distinct object-aware features, handles sparse scenes well and reduces computational burden [22].

3D Single object tracking. Recently, with the rapid development of sensors, 3D sensors such as LiDAR can obtain 3D point cloud data for 3D single object tracking. Giancola *et al.* [7] first proposed a shape-completion-based 3D Siamese tracker (SC3D), which originally encodes shape information into the template for matching template and search area. However, SC3D cannot be end-to-end trained. Qi *et al.* [23] proposed a point-to-box (P2B) Siamese tracking scheme, which adopted the target-specific feature augmentation module to learn template and search area cross-correlation and utilized Hough Voting modules to regress potential target centers in the search area. Zhou *et al.* [34] proposed PTTR that firstly adopted relation-aware sampling (RAS) in the Siamese network, search area branch obtains a feature map shared by the template for sampling reference, which effectively preserves object points in the search area. Furthermore, Hui *et al.* [8] proposed a novel BBox regression module, which compressed voxelized sparse 3D features for 2D detection and performs effective object tracking.

Object segmentation. Object-preserved sampling employed in OPSNet is similar to object segmentation, but they differ in task-driven purposes. Recently proposed object segmentation approaches [1, 17, 19, 24] are based on deep learning. Wu *et al.* [28] formulated object segmentation as a point-wise multi-class classification problem, and they propose an end-to-end pipeline called SqueezeSeg based on convolutional neural networks. Our object-preserved sampling also aims at point-wise classification, but the task-driven purpose is selecting object candidates by referring to the point-wise highlighting scores.

3. Method

3.1. Overview

In Siamese-based tracking methods, the backbone down-samples template and search area to obtain their seeds by set abstraction layers that consist of sampling and grouping [22], each seed is represented as $[x; f] \in \mathbb{R}^{3+d_1}$, where x denotes the 3D coordinates of the seed and f is the seed features vector. We aim to retain object points by object-preserved sampling and highlight object-aware features in the search area for accurate object localization. OPSNet

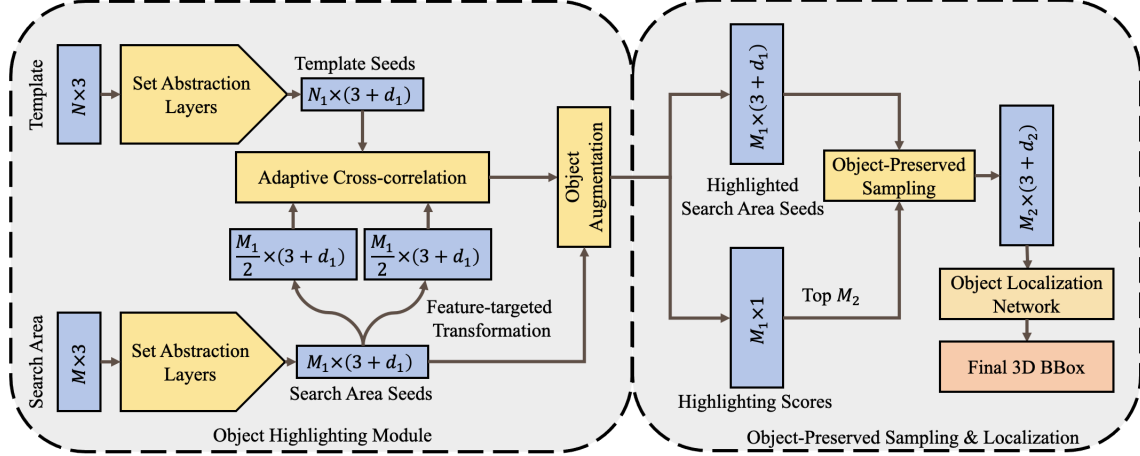


Figure 2. The main pipeline of OPSNet. OPSNet consists of two main parts: 1) object highlighting module, and 2) object-preserved sampling and localization. Firstly, the set abstraction layers output template and search area seeds, respectively. Then, with the help of template seeds object highlighting module enhances the object-aware features and extracts the discriminative features from search area seeds. Finally, the object-preserved sampling selects object candidates from the highlighted search area seeds for object preservation and accurate 3D BBox localization.

has two main parts (Fig. 2): 1) object highlighting module, and 2) object-preserved sampling and localization. The object highlighting module aims to enhance object-aware features and extract discriminative features from template and search area, which can assist the object-preserved sampling to achieve object-background recognition. Object-preserved sampling and localization maintain object integrity and reduce redundancy for effectively predicting accurate BBoxes.

3.2. Object Highlighting Module

Raw points in template P_{tmp} (of size N) and search area P_{sea} (of size M) are fed into a feature backbone to obtain N_1 template seeds $Q = \{q_i\}_{i=1}^{N_1}$ and search area seeds $R = \{r_j\}_{j=1}^{M_1}$, the backbone consists of two set abstraction layers. Then feature-targeted transformation module converts the search area seeds into two feature-targeted seed subsets. After that, the adaptive cross-correlation utilizes two branches to respectively handle two subsets, one branch highlights object-aware features with consistent cross-correlation; the other branch extracts discriminative features with discrepant cross-correlation. Finally, the object augmentation module further enhances the object-aware features.

Feature-targeted transformation. Feature-targeted transformation initializes two independent MLPs with input and output dimension $\{M_1, \frac{M_1}{2}\}$, then the transposed search area seeds R^T are fed into them to generate two feature-targeted seed subsets R_1^T and R_2^T , respectively. For dimension alignment, we transpose R_1^T and R_2^T to obtain feature-targeted subsets R_1 (of size $\frac{M_1}{2}$) and R_2 (of size $\frac{M_1}{2}$).

Adaptive Cross-correlation. Adaptive cross-correlation

consists of consistent and discrepant cross-correlation.

Consistent cross-correlation. Consistent cross-correlation computes the cosine similarity F_{cos} between a seed subset R_1 and the template seeds Q , which focuses more on consistent semantic correlation.

$$s_{ij} = F_{cos}(q_i, r_j) = \frac{q_i^T \cdot r_j}{\|q_i\|_2 \cdot \|r_j\|_2} \quad (1)$$

where q_i, r_j respectively denotes certain point in template seeds Q and feature-targeted subset R_1 . s_{ij} denotes the cosine similarity between points q_i, r_j . Then we gather the most similar point in template seeds with each point in the subset R_1 , as Fig. 3 shows, which can be written as :

$$r_j' = \text{MLP}[r_j, s_{kj}, q_k, x_k] \\ k = \underset{i=1,2,\dots,N_1}{\text{argmax}} \{F_{cos}(q_i, r_j)\}, \forall r_j \in R_1 \quad (2)$$

where k is the index of the maximum similarity $F_{cos}(q_i, r_j)$ value, and s_{kj}, x_k are the corresponding maximum value and coordinate (x, y, z) , respectively. $[\cdot, \cdot, \cdot, \cdot]$ denotes concatenation.

Here, we obtain a consistent cross-correlated feature vector r_j' of j -th point in the subset R_1 after MLP and integrate them to generate consistent cross-correlated seeds subset R_1' .

Discrepant cross-correlation. Discrepant cross-correlation extracts discrepant semantics between Q and feature-targeted subset R_2 into R_2 . We firstly learn a discrepancy map by computing subtracted difference and using an MLP, which is formulated as:

$$d_{ij} = F_{sub}(q_i, r_j) = \text{MLP}(q_i - r_j), \forall q_i \in Q, r_j \in R_2 \quad (3)$$

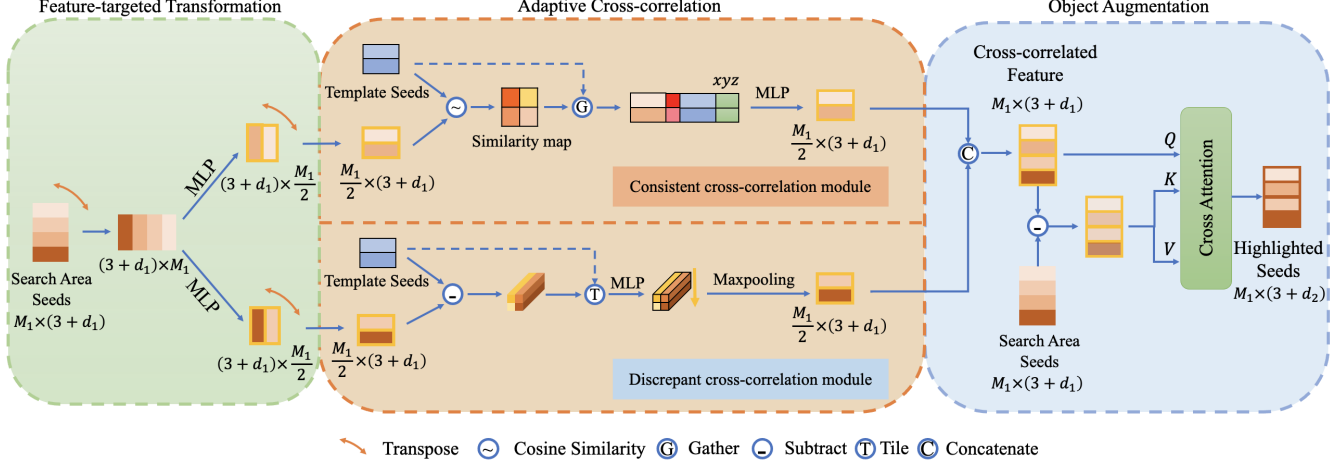


Figure 3. Illustration of the object highlighting module. Object highlighting module can be divided into three main parts: 1) feature-targeted transformation converts search area seeds into two feature-targeted seed subsets, 2) adaptive cross-correlation extracts the consistent and discrepant features into two subsets respectively with the help of the template seeds, 3) object augmentation further enhances the object features by employing the cross attention mechanism.

where q_i, r_j respectively denote certain point in the template seeds Q and subset R_2 . d_{ij} denotes the discrepant weight between points q_i, r_j , as Fig. 3 shows. The discrepant cross-correlated targeted point r_j'' is given by:

$$r_j'' = \text{MLP}\left(\text{MAX}_{i=1,2,\dots,N_1} \{q_i \cdot d_{ij}\}\right) \quad (4)$$

here MAX is the max pooling operator. We obtain a discrepant cross-correlated feature vector r_j'' of j -th point in the subset R_2 and integrate them to generate discrepant cross-correlated seeds subset R_2' .

Concatenating R_1' and R_2' , the cross-correlated search area seeds R' are obtained.

Object augmentation. We first subtract the cross-correlated seeds R' and search area seeds R , then put the subtracted tensor into MLP for augmenting differentiation features R^Δ . For further augmenting the object-aware features in the cross-correlated seeds R' , cross attention mechanism is adopted, which can be formulated as:

$$\tilde{R} = \text{CrossAttention}(R' + X^s, R^\Delta + X^s, R^\Delta + X^s) \quad (5)$$

where the three inputs from left to right are used as query, key, and value in Eq. (5), respectively. X^s denotes the position embedding.

Here the object-highlighted search area seeds $\tilde{R} = \{f_j\}_{j=1}^{M_1}$ are obtained.

3.3. Object Preserved Sampling

Obtained object-highlighted search area seeds $\tilde{R} = \{f_j\}_{j=1}^{M_1}$ and given original BBox annotations, point-wise

one-hot labels $Y = \{y_i\}_{i=1}^{M_1}$ can be generated. We predict a highlighting score for each seed: $\hat{y}_i = \text{MLP}(f_i)$, $i = 1, 2, \dots, M_1$, and select seeds with highest M_2 scores as candidates. In addition, smooth one-hot labels is formulated as:

$$y_i' = \begin{cases} y_i - \frac{\epsilon}{M_1}, & y_i = 1. \\ y_i + \frac{\epsilon}{M_1}, & y_i = 0. \end{cases} \quad (6)$$

Obtained the smooth one-hot labels, we compute the Focal loss [14] for supervision. Considering the search area generally contains unbalanced objects and background points number, the focal loss can be regarded as an ingenious solution, which is defined by:

$$\mathcal{L}_{cls} = - \sum y_i' [y_i = 1] (1 - \hat{y}_i)^\alpha \log(\hat{y}_i) + y_i' [y_i = 0] \hat{y}_i^\alpha \log(1 - \hat{y}_i) \quad (7)$$

where $y_i'[\text{cond.}]$ is the indicator function, follows Eq. (6), \hat{y}_i is the predicted highlighting score. Besides, $\alpha = 2$ is empirically set in all experiments.

We select object candidates with top M_2 highlighting scores as ball query centers for grouping and aggregating local features to obtain object-preserved search area seeds $R^{op} = \{r_j^{op}\}_{j=1}^{M_2}$, $r_j^{op} = [x_j^{op}, f_j^{op}] \in \mathbb{R}^{3+d_2}$, where x^{op} denotes the object-preserved seed coordinates and f^{op} is the feature vector.

3.4. Object Localization Network

Inspired by [5, 8], we develop an object localization network utilizing bird's eyes view (BEV), and the object detection paradigm has been customized for tracking adaption.

Firstly, sparse search area seeds R^{op} requires to be segmented within the BEV range

$[(x_{min}, x_{max}), (y_{min}, y_{max})]$. We voxelize segmented R^{op} with voxel side length as r , then we can obtain dense BEV feature map $\mathcal{E} \in \mathbb{R}^{H \times W \times c}$ in x - y plane, where $H = \lfloor \frac{x_{max} - x_{min}}{r} \rfloor$, $W = \lfloor \frac{y_{max} - y_{min}}{r} \rfloor$, and c is the channel of features that obtained by average pooling. Then we locate the original 3D point coordinates (x, y, z) in 2D x - y plane presented by (u, v) , where $u = \frac{x - x_{min}}{r}$ and $v = \frac{y - y_{min}}{r}$. Since the dense map uses discrete coordinates, we need discrete $(\bar{u}, \bar{v}) = (\lfloor u \rfloor, \lfloor v \rfloor)$ as well. Here $\lfloor \cdot \rfloor$ denotes floor operation.

Therefore, we can localize 2D-center based on the dense BEV feature map, we discretize ground truth bounding box (GTBB) center $p^c(x, y, z)$ into $p^c(\bar{u}, \bar{v})$, then we expand p^c into a center map $\mathcal{M} \in \mathbb{R}^{H \times W \times 1}$ that defined by:

$$\begin{cases} p_{ij} = \frac{1}{d+1}, & p_{ij} \in \mathbf{B}. \\ p_{ij} = 0, & p_{ij} \notin \mathbf{B}. \end{cases} \quad (8)$$

where d presents the Euclidean distance between p_{ij} and GTBB center p^c ; $p_{ij} \in \mathbf{B}$ and $p_{ij} \notin \mathbf{B}$ mean the pixel p_{ij} inside or outside the 2D GTBB \mathbf{B} , respectively.

Pervasive distractors can easily mislead object center localization, and we need to localize the only object required to track with, thus we conduct train & test syncretic loss punishment on wrongly located centers. We firstly predict n stacked center maps $\hat{\mathcal{M}}_n \in \mathbb{R}^{H \times W \times n}$ from BEV feature map \mathcal{E} but we only enforce the first center map $\hat{\mathcal{M}}_0 \in \mathbb{R}^{H \times W \times 1}$ to approach the ground truth \mathcal{M} by using Focal loss [14], which denoted by \mathcal{L}_{center} . As for other $n - 1$ center maps, we compute Euclidean distances summation between the predicted centers \hat{p}_i^c in $\hat{\mathcal{M}}_i, (i = 1, 2, \dots, n)$ and GT, which is defined by:

$$\mathcal{L}_{loc} = \frac{1}{n} \sum_{i=1}^k \|p^c - \hat{p}_i^c\|_2 \quad (9)$$

where \hat{p}_i^c denotes i -th predicted center in $\hat{\mathcal{M}}_i$.

Since the 2D BEV-based feature map generates a discrete 2D-center, the offset of the continuous ground truth center requires to be regressed. We surround the predicted object center with a square of radius l . Similar to 2D-center prediction, predicted offset map $\hat{\mathcal{O}} \in \mathbb{R}^{H \times W \times 2}$ is generated from BEV feature map \mathcal{E} , which is supervised by:

$$\mathcal{L}_{off} = \sum_{\delta x=-l}^l \sum_{\delta y=-l}^l |\hat{\mathcal{O}}_{p^c+(\delta x, \delta y)} - [\tilde{p}^c - p^c + (\delta x, \delta y)]| \quad (10)$$

where \tilde{p}^c and p^c present the ground truth center with continuous and discrete coordinates respectively.

Two individual CNNs are applied to directly regress the z -axis coordinate and the rotation angle θ . Given two predicted z -axis map $\hat{\mathcal{Z}} \in \mathbb{R}^{H \times W \times 1}$ and the rotation map

$\hat{\Theta} \in \mathbb{R}^{H \times W \times 1}$, we use L_1 loss to compute error:

$$\mathcal{L}_z = |\hat{\mathcal{Z}}_c - z| \quad (11)$$

$$\mathcal{L}_\theta = |\hat{\Theta} - \theta| \quad (12)$$

We sum the all above losses as our final network loss: $\mathcal{L} = \lambda_1(\mathcal{L}_{center} + \mathcal{L}_{loc} + \mathcal{L}_{off} + \mathcal{L}_\theta) + \lambda_2\mathcal{L}_z + \lambda_3\mathcal{L}_{cls}$. λ_1, λ_2 , and λ_3 are the hyper-parameters for loss regulation.

4. Experiments

Extensive experiments have been conducted to validate the effectiveness of our OPSNet and its components, we mainly focus on car and pedestrian tracking since cars and pedestrians appear in large quantity and diversity.

4.1. Experimental Settings

Datasets. KITTI [6] and Waymo Open Dataset (WOD) [25] are used for training and validation. Since the labels of the KITTI test set are not provided, following previous works [7, 23, 32], we use the training set to train and evaluate. The training set is spilt as follows: scenes 0-16 for training, scenes 17-18 for validation, and scenes 19-20 for testing. For WOD, we follow [34] to transform the WOD into class-balanced tracklets that tracking paradigms can handle. **Evaluation Metrics.** Our evaluation metrics use the One Pass Evaluation (OPE) [29] from single object tracking. The Success metrics are defined as the Area Under Curve (AUC) of the IoU between the predicted box and the GT. The Precision metrics are defined as the AUC of the distance between the centers for errors from 0 to 2m.

Implementation details. Following [23], template number of points sets as $N = 512$ and search area sets as $M = 1024$ by randomly points discarding and duplicating. We obtain template and search area seeds by three set abstraction layers with query radii of 0.3, 0.5, and 0.7, yielding $M_1 = 256$, $N_1 = 128$ and we set the seed feature dimension $d_1 = 128$. Object-preserved sampling selects highlighted search area seeds with top 128 scores, yielding $M_2 = 128$, and local feature aggregation generates object-preserved seeds with feature dimension $d_2 = 128$.

Targeted-feature transformation module uses two 3-layer MLPs with batch normalization (BN) and a ReLU activation layer. For highlighting score prediction, object preserved sampling uses 3-layer MLP and Sigmoid function for object score prediction. In the object localization network, we set the voxel side length $r = 0.3\text{m}$, the channel of BEV feature map $c = 128$, and we generate 4 stacked center maps ($n = 4$). For loss regulation, we set $\lambda_1 = 1.0$, $\lambda_2 = 2.0$, and $\lambda_3 = 0.5$.

Training and testing. We aggregate the first GTBB of the current tracklet and the previous GTBB as the template, which is applied with a random offset on the previous GTBB to augment data. The search areas are augmented

Table 1. Comparison with other state-of-the-art approaches on the KITTI dataset. The instance frame number of each category is shown under category names, and the mean denotes the average results of all categories. Bold presents the best performance.

Category	Car	Ped	Van	Cyclist	Mean	
Frame num.	6424	6088	1248	308	14068	
Success	P2B [23]	56.2	40.8	40.8	32.1	39.5
	BAT [32]	60.5	42.1	52.4	33.7	47.2
	LTTR [3]	65.0	33.2	35.8	66.2	50.0
	V2B [8]	70.5	48.3	50.1	40.8	58.4
	PTTR [34]	65.2	50.9	52.5	65.1	58.4
	STNet [9]	72.1	49.9	58.0	73.5	61.3
	M2-Track [33]	65.5	61.5	53.8	73.2	62.9
	OPSNet (ours)	77.0	65.6	77.7	85.5	72.3
	Precision	P2B [23]	72.8	49.6	48.4	44.7
BAT [32]		77.7	70.1	67.0	45.4	65.1
LTTR [3]		77.1	56.8	45.6	89.9	67.4
V2B [8]		81.3	73.5	58.0	49.7	75.2
PTTR [34]		77.4	81.6	61.8	90.5	77.8
STNet [9]		84.0	77.2	70.6	93.7	80.1
M2-Track [33]		80.8	88.2	70.7	93.5	83.4
OPSNet (ours)		86.1	90.3	85.8	93.7	88.0

similarly by enlarging the current GT with an offset, for all experiments, this offset sets as 2m. Additionally, we apply the Adam optimizer [12] with an initial learning rate of 0.001 and decreased by 5 times after 10 epochs. We train the OPSNet on a single NVIDIA RTX2080 Ti GPU with a batchsize of 32. OPSNet can obtain satisfying results after about 40 epochs.

4.2. Results

Evaluation on KITTI. As shown in Tab. 1, our OPSNet shows a large improvement over SOTA methods, All the methods besides M2-track [33] apply the Siamese-based network. Our OPSNet outperforms the SOTA tracking paradigm M2-track with a large margin of $\sim 9.4\%$ / $\sim 4.6\%$ on average success / precision and the SOTA PTTR [34] based on PointNet++ of $\sim 13.9\%$ / $\sim 10.2\%$. Our OPSNet achieves the highest tracking performance in all four categories. As shown in Fig. 4, we compare the proposed OPSNet against PTTR over the car and pedestrian sequences since PTTR adopts relation-aware sampling for object preservation. The error gradually accumulates in PTTR tracking since the bad template misleads the search area sampling, but the object-preserved search area seeds generated by object-preserved sampling assist the OPSNet to perform robust tracking.

Evaluation on WOD. To validate the generalization ability of our OPSNet, we use our OPSNet that pre-trained over the KITTI dataset for testing tracking on Waymo Open Dataset (WOD) following [8]. According to the point number of the first frame, WOD can be divided into three subsets of different tracking levels of difficulty, including easy, medium,

Table 2. Comparison with other state-of-the-art approaches on the WOD dataset.

Category	Vehicle				
Level	Easy	Medium	Hard	Mean	
Frame num.	67832	61252	56647	185371	
Success	BAT [32]	61.0	53.3	48.9	54.7
	V2B [8]	64.5	55.1	52.0	57.6
	STNet [9]	65.9	57.5	54.6	59.7
	OPSNet (ours)	68.8	58.7	55.2	61.3
Precision	BAT [32]	68.3	60.9	57.8	62.7
	V2B [8]	71.5	63.2	62.0	65.9
	STNet [9]	72.7	66.0	64.7	68.0
	OPSNet (ours)	74.4	66.9	65.1	69.1
Category	Pedestrian				
Level	Easy	Medium	Hard	Mean	
Frame num.	85280	82253	74219	241752	
Success	BAT [32]	19.3	17.8	17.2	18.2
	V2B [8]	27.9	22.5	20.1	23.7
	STNet [9]	29.2	24.7	22.2	25.5
	OPSNet (ours)	32.2	28.4	25.1	28.7
Precision	BAT [32]	32.6	29.8	28.3	30.3
	V2B [8]	43.9	36.2	33.1	37.9
	STNet [9]	45.3	38.2	35.8	39.9
	OPSNet (ours)	47.4	41.9	37.6	42.5

and hard. Even though tracking frames are far more than KITTI has, our OPSNet still shows the generalization ability of the tracking performance on WOD, which outperforms the baseline BAT [32] with a gain of $\sim 6.6\%$ / $\sim 6.4\%$ on the category Vehicle, results as Tab. 2 shows.

Tracking on sparse point clouds. Handling extreme sparse scenes is a great challenge in 3D SOT tasks. We test our OPSNet on the object of extreme sparse points, which is divided into three object point number intervals including $[0, 50)$, $[50, 100)$, $[100, 150)$. We compare the tracking result of our OPSNet, PTTR [34], V2B [8], and STNet [9]. As Fig. 5 shows, our OPSNet achieves the highest tracking performance on three intervals with $\sim 2.8\%$ / $\sim 2.6\%$, $\sim 4.7\%$ / $\sim 3.7\%$, $\sim 6.7\%$ / $\sim 4.7\%$ success / precision gain over the V2B. Experiment results demonstrate that our OPSNet effectively preserves sparse objects and handles extreme sparse point clouds well.

Tracking on long sequences. Siamese-based methods probably lose the object when tracking on long sequences. Therefore the performance on long sequences evaluates the robustness of SOT methods. PTTR adopts their relation-aware sampling for object preservation, therefore we test our OPSNet and PTTR on sequence length intervals $[0, 50)$, $[50, 200)$, $[200, +\infty)$ and compute average recall rate after sampling as the indicator of object preservation. As Fig. 6 shows, our OPSNet outperforms the PTTR on three intervals with $\sim 11.8\%$ / $\sim 7.7\%$, $\sim 10.1\%$ / $\sim 6.4\%$,

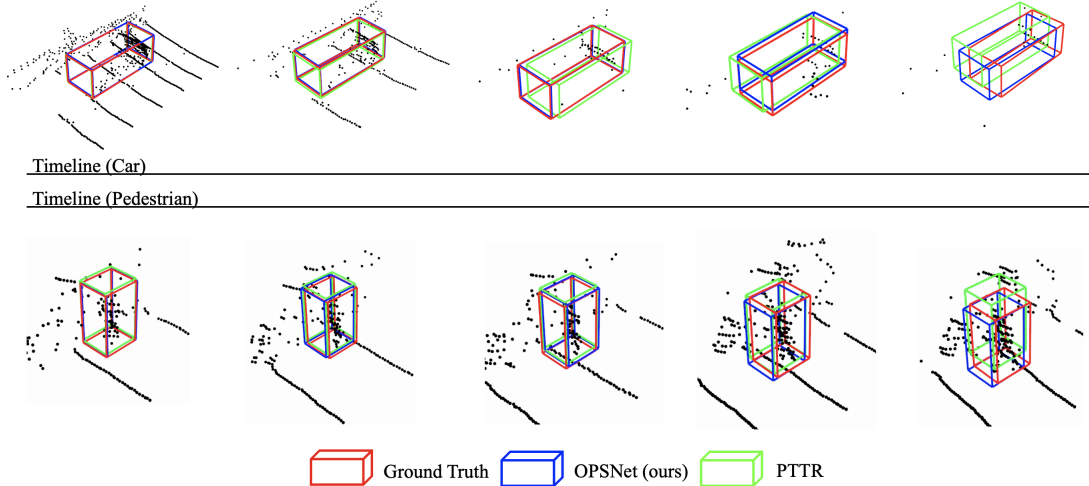


Figure 4. Result comparison visualization with PTTR [34]. We can observe that the predicted BBoxes by OPSNet hold tight to the ground truths.

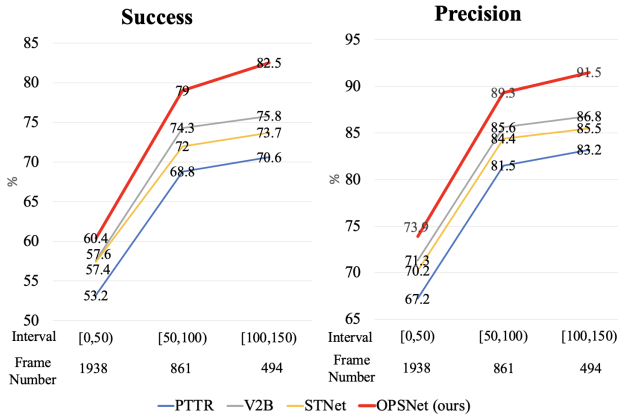


Figure 5. Evaluated mean success / precision of the three extreme sparse point number intervals on the KITTI Car category.

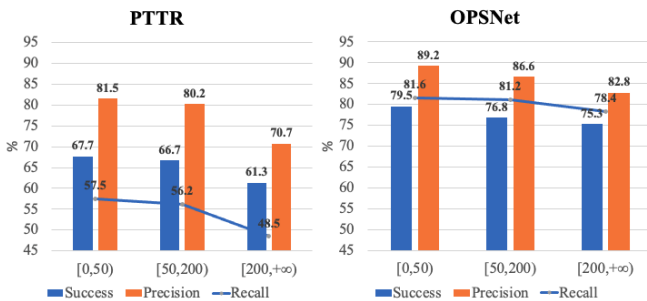


Figure 6. Evaluated mean success / precision and recall rate of the three sequence length intervals on the KITTI Car category.

$\sim 14.0\%$ / $\sim 12.1\%$ success / precision gain and $\sim 22.0\%$, $\sim 20.6\%$, $\sim 29.9\%$ recall rate gain.

Running speed. We evaluate the inference speed of our

model on a single RTX2080 Ti GPU. Our method achieves 23 FPS, including 21 ms for pre-processing point clouds, 21 ms for network forward propagation, and 2 ms for post-processing. We also test V2B, and STNet in the default settings run with 20 FPS and 19 FPS, respectively.

4.3. Ablation Studies

We conduct ablation studies to evaluate the modules proposed in OPSNet, the results are shown with OPE evaluation metrics and based on the KITTI dataset.

Comparison on sampling strategies. We compare our proposed object preserved sampling (OPS) with existing unsupervised sampling strategies including relation-aware sampling (RAS) [34], random sampling (RS) [23], and furthest point sampling (FPS) [22] on sampling 128 candidates from the 256 search area seeds, as Fig. 7 shows. We compute the recall rates for object points after sampling which demonstrate the effectiveness of our OPS. We also replace our OPS with RAS, RS, and FPS in OPSNet, default OPSNet outperforms clear success / precision gain of $\sim 4.7\%$ / $\sim 3.6\%$ on the car category and $\sim 9.0\%$ / $\sim 8.8\%$ on the pedestrian over the FPS baseline, comparison shown in Tab. 3.

Ablation studies on object highlighting module. We conduct ablation experiments to validate the effectiveness of the object highlighting components, respectively, as Tab. 4 shows. We report the results of cars and pedestrians tracking on the KITTI dataset. Only a single cross-correlation approach cannot perform the best tracking ($\sim 6.9\%$ / $\sim 3.5\%$ decrease with only consistent cross-correlation and $\sim 6.4\%$ / $\sim 3.0\%$ decrease with only discrepant cross-correlation on Car). For analyzing feature-targeted transformation, we simply divide the search area into two subsets without utilizing MLPs, so that the cross-correlation cannot be adap-

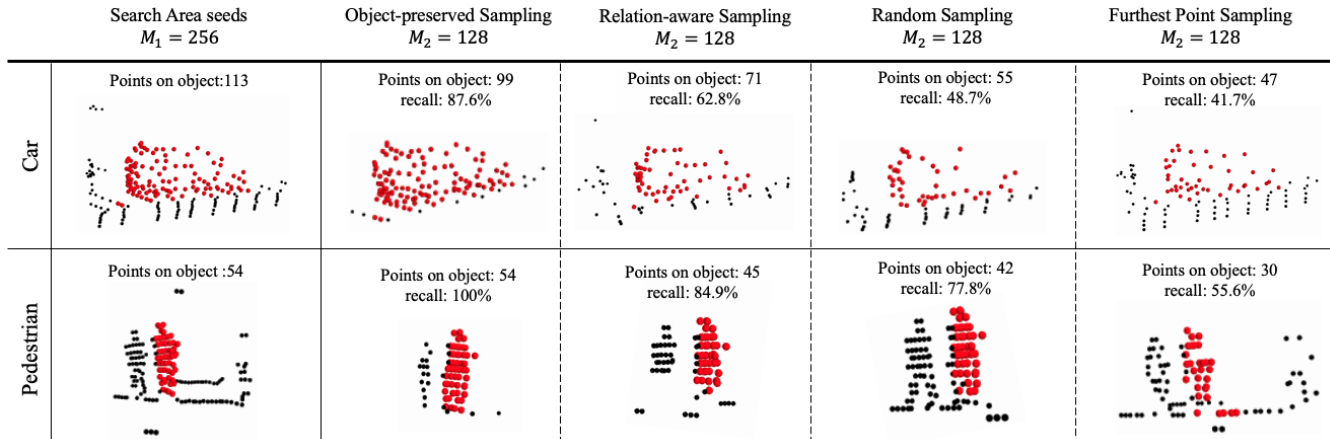


Figure 7. Comparison on sampling strategies: our object-preserved sampling (OPS), relation-aware sampling (RAS) proposed in PTTR [34], random sampling (RS) employed in [23], and furthest points sampling (FPS) proposed in PointNet++ [22]. Note that red points denote the object and black ones denote the background.

Table 3. Tracking performance comparison on different sampling approaches. Shown by the evaluation metrics success / precision on the category car and pedestrian.

Method	Car	Pedestrian
RS [23]	72.9 / 83.7	58.2 / 82.1
FPS [22]	71.2 / 81.8	52.4 / 80.5
RAS [34]	73.3 / 83.0	61.0 / 84.5
OPS (ours)	77.0 / 86.1	65.6 / 90.3

Table 4. Ablation studies results on object highlighting module.

	Car	Pedestrian
w/o object augmentation	74.5 / 84.3	62.2 / 86.9
w/o feature-targeted transformation	69.3 / 82.5	59.1 / 79.8
only consistent cross-correlation	70.1 / 82.6	59.9 / 80.1
only discrepant cross-correlation	70.6 / 83.1	60.3 / 80.5
default setting	77.0 / 86.1	65.6 / 90.3

tively conducted ($\sim 7.7\%$ / $\sim 3.6\%$ decrease without the feature-targeted transformation on Car). Results demonstrate that object augmentation further improves tracking performance ($\sim 2.5\%$ / $\sim 1.8\%$ gain on the category Car).

Ablation studies on object localization network. We replace our object localization network (OLN) with the VoteNet-based approaches including Region Proposal Network (RPN) applied in [23, 32] and coarse-to-refine regression (C2R) proposed in [34] to validate the tracking performance. VoteNet regresses the offset from point to center with a score as proposals. However, when facing sparse scenes VoteNet is hard to generate high-quality proposals.

Table 5. Tracking performance comparison on common object locating approaches.

	Car	Pedestrian
RPN [23, 32]	68.0 / 79.6	48.8 / 72.5
C2R [34]	71.5 / 83.2	57.1 / 80.2
OLN (ours)	77.0 / 86.1	65.6 / 90.3

Our object localization network does not require generating numerous 3D proposals thus it can handle the above issue and outperforms baseline RPN with $\sim 9.0\%$ / $\sim 6.5\%$ and $\sim 16.8\%$ / $\sim 17.8\%$ increase on the category Car and Pedestrian.

5. Conclusion

In this paper, we propose a novel Object Preserving Siamese Network (OPSNet) for single object tracking on point clouds. Our OPSNet aims to enhance the object-aware features and extract discriminative features from template and search area with the object highlighting module, maintain object integrity and drop redundant background points with the object-preserved sampling, and predict accurate BBoxes with the object localization network.

The experimental results ($\sim 9.4\%$ and $\sim 2.5\%$ success gain on KITTI and WOD respectively) demonstrate that our OPSNet achieves high-performance object tracking and possesses generalization ability, indicate that object highlighting module and object-preserved sampling effectively handle sparse point clouds and assist the object localization network to perform robust tracking on long sequences.

References

- [1] Tristan Brodeur, Hadi AliAkbarpour, and Steve Sudderth. Point cloud object segmentation using multi elevation-layer 2d bounding-boxes. In *Proceedings of the IEEE/CVF International Conference on Computer Vision*, pages 3917–3925, 2021. 2
- [2] Widodo Budiharto, Edy Irwansyah, Jarot Sembodo Suroso, and Alexander Agung Santoso Gunawan. Design of object tracking for military robot using pid controller and computer vision. *ICIC Express Letters*, 14(3):289–294, 2020. 1
- [3] Yubo Cui, Zheng Fang, Jiayao Shan, Zuoxu Gu, and Sifan Zhou. 3d object tracking with transformer. *arXiv preprint arXiv:2110.14921*, 2021. 6
- [4] Zhipeng Ding, Xu Han, and Marc Niethammer. Votenet: A deep learning label fusion method for multi-atlas segmentation. In *International Conference on Medical Image Computing and Computer-Assisted Intervention*, pages 202–210. Springer, 2019. 2
- [5] Runzhou Ge, Zhuangzhuang Ding, Yihan Hu, Yu Wang, Sijia Chen, Li Huang, and Yuan Li. Afdet: Anchor free one stage 3d object detection. *arXiv preprint arXiv:2006.12671*, 2020. 4
- [6] Andreas Geiger, Philip Lenz, and Raquel Urtasun. Are we ready for autonomous driving? the kitti vision benchmark suite. In *2012 IEEE conference on computer vision and pattern recognition*, pages 3354–3361. IEEE, 2012. 2, 5
- [7] Silvio Giancola, Jesus Zarzar, and Bernard Ghanem. Leveraging shape completion for 3d siamese tracking. In *Proceedings of the IEEE/CVF Conference on Computer Vision and Pattern Recognition*, pages 1359–1368, 2019. 1, 2, 5
- [8] Le Hui, Lingpeng Wang, Mingmei Cheng, Jin Xie, and Jian Yang. 3d siamese voxel-to-bev tracker for sparse point clouds. *Advances in Neural Information Processing Systems*, 34:28714–28727, 2021. 1, 2, 4, 6
- [9] Le Hui, Lingpeng Wang, Linghua Tang, Kaihao Lan, Jin Xie, and Jian Yang. 3d siamese transformer network for single object tracking on point clouds. *arXiv preprint arXiv:2207.11995*, 2022. 1, 6
- [10] Anastasia Ioannidou, Elisavet Chatzilari, Spiros Nikolopoulos, and Ioannis Kompatsiaris. Deep learning advances in computer vision with 3d data: A survey. *ACM computing surveys (CSUR)*, 50(2):1–38, 2017. 1
- [11] Muxi Jiang, Rui Li, Qisheng Liu, Yingjing Shi, and Esteban Tlelo-Cuautle. High speed long-term visual object tracking algorithm for real robot systems. *Neurocomputing*, 434:268–284, 2021. 1
- [12] Diederik P Kingma and Jimmy Ba. Adam: A method for stochastic optimization. *arXiv preprint arXiv:1412.6980*, 2014. 6
- [13] Alex H Lang, Sourabh Vora, Holger Caesar, Lubing Zhou, Jiong Yang, and Oscar Beijbom. Pointpillars: Fast encoders for object detection from point clouds. In *Proceedings of the IEEE/CVF conference on computer vision and pattern recognition*, pages 12697–12705, 2019. 2
- [14] Tsung-Yi Lin, Priya Goyal, Ross Girshick, Kaiming He, and Piotr Dollár. Focal loss for dense object detection. In *Proceedings of the IEEE international conference on computer vision*, pages 2980–2988, 2017. 2, 4, 5
- [15] Zhe Liu, Chuangzhe Suo, Yingtian Liu, Yueling Shen, Zhijian Qiao, Huanshu Wei, Shunbo Zhou, Haoang Li, Xinwu Liang, Hesheng Wang, et al. Deep learning-based localization and perception systems: approaches for autonomous cargo transportation vehicles in large-scale, semiclosed environments. *IEEE Robotics & Automation Magazine*, 27(2):139–150, 2020. 1
- [16] Yuzhen Lu and Sierra Young. A survey of public datasets for computer vision tasks in precision agriculture. *Computers and Electronics in Agriculture*, 178:105760, 2020. 1
- [17] Huan Luo, Quan Zheng, Lina Fang, Yingya Guo, Wenzhong Guo, Cheng Wang, and Jonathan Li. Boundary-aware graph markov neural network for semiautomated object segmentation from point clouds. *International Journal of Applied Earth Observation and Geoinformation*, 104:102564, 2021. 2
- [18] Wenjie Luo, Bin Yang, and Raquel Urtasun. Fast and furious: Real time end-to-end 3d detection, tracking and motion forecasting with a single convolutional net. In *Proceedings of the IEEE conference on Computer Vision and Pattern Recognition*, pages 3569–3577, 2018. 1
- [19] Lingfei Ma, Ying Li, Jonathan Li, Weikai Tan, Yongtao Yu, and Michael A Chapman. Multi-scale point-wise convolutional neural networks for 3d object segmentation from lidar point clouds in large-scale environments. *IEEE Transactions on Intelligent Transportation Systems*, 22(2):821–836, 2019. 2
- [20] Mattia Natali, Silvia Biasotti, Giuseppe Patanè, and Bianca Falcidieno. Graph-based representations of point clouds. *Graphical Models*, 73(5):151–164, 2011. 2
- [21] Charles R Qi, Hao Su, Kaichun Mo, and Leonidas J Guibas. Pointnet: Deep learning on point sets for 3d classification and segmentation. In *Proceedings of the IEEE conference on computer vision and pattern recognition*, pages 652–660, 2017. 2
- [22] Charles Ruizhongtai Qi, Li Yi, Hao Su, and Leonidas J Guibas. Pointnet++: Deep hierarchical feature learning on point sets in a metric space. *Advances in neural information processing systems*, 30, 2017. 1, 2, 7, 8
- [23] Haozhe Qi, Chen Feng, Zhiguo Cao, Feng Zhao, and Yang Xiao. P2b: Point-to-box network for 3d object tracking in point clouds. In *Proceedings of the IEEE/CVF Conference on Computer Vision and Pattern Recognition*, pages 6329–6338, 2020. 1, 2, 5, 6, 7, 8
- [24] Ziyang Song and Bo Yang. Ogc: Unsupervised 3d object segmentation from rigid dynamics of point clouds. *arXiv preprint arXiv:2210.04458*, 2022. 2
- [25] Pei Sun, Henrik Kretzschmar, Xerxes Dotiwalla, Aurelien Chouard, Vijaysai Patnaik, Paul Tsui, James Guo, Yin Zhou, Yuning Chai, Benjamin Caine, et al. Scalability in perception for autonomous driving: Waymo open dataset. In *Proceedings of the IEEE/CVF conference on computer vision and pattern recognition*, pages 2446–2454, 2020. 2, 5
- [26] Siyu Tang, Mykhaylo Andriluka, Bjoern Andres, and Bernt Schiele. Multiple people tracking by lifted multicut and person re-identification. In *Proceedings of the IEEE conference*

- on computer vision and pattern recognition, pages 3539–3548, 2017. [1](#)
- [27] Yue Wang, Yongbin Sun, Ziwei Liu, Sanjay E Sarma, Michael M Bronstein, and Justin M Solomon. Dynamic graph cnn for learning on point clouds. *Acm Transactions On Graphics (tog)*, 38(5):1–12, 2019. [2](#)
- [28] Bichen Wu, Alvin Wan, Xiangyu Yue, and Kurt Keutzer. Squeezeseg: Convolutional neural nets with recurrent crf for real-time road-object segmentation from 3d lidar point cloud. In *2018 IEEE International Conference on Robotics and Automation (ICRA)*, pages 1887–1893, 2018. [2](#)
- [29] Yi Wu, Jongwoo Lim, and Ming-Hsuan Yang. Online object tracking: A benchmark. In *Proceedings of the IEEE conference on computer vision and pattern recognition*, pages 2411–2418, 2013. [5](#)
- [30] Junliang Xing, Haizhou Ai, and Shihong Lao. Multiple human tracking based on multi-view upper-body detection and discriminative learning. In *2010 20th International Conference on Pattern Recognition*, pages 1698–1701. IEEE, 2010. [1](#)
- [31] Zetong Yang, Yanan Sun, Shu Liu, and Jiaya Jia. 3dssd: Point-based 3d single stage object detector. In *Proceedings of the IEEE/CVF conference on computer vision and pattern recognition*, pages 11040–11048, 2020. [2](#)
- [32] Chaoda Zheng, Xu Yan, Jiantao Gao, Weibing Zhao, Wei Zhang, Zhen Li, and Shuguang Cui. Box-aware feature enhancement for single object tracking on point clouds. In *Proceedings of the IEEE/CVF International Conference on Computer Vision*, pages 13199–13208, 2021. [1](#), [5](#), [6](#), [8](#)
- [33] Chaoda Zheng, Xu Yan, Haiming Zhang, Baoyuan Wang, Shenghui Cheng, Shuguang Cui, and Zhen Li. Beyond 3d siamese tracking: A motion-centric paradigm for 3d single object tracking in point clouds. In *Proceedings of the IEEE/CVF Conference on Computer Vision and Pattern Recognition*, pages 8111–8120, 2022. [6](#)
- [34] Changqing Zhou, Zhipeng Luo, Yueru Luo, Tianrui Liu, Liang Pan, Zhongang Cai, Haiyu Zhao, and Shijian Lu. Pptr: Relational 3d point cloud object tracking with transformer. In *Proceedings of the IEEE/CVF Conference on Computer Vision and Pattern Recognition*, pages 8531–8540, 2022. [1](#), [2](#), [5](#), [6](#), [7](#), [8](#)
- [35] Yin Zhou and Oncel Tuzel. Voxelnet: End-to-end learning for point cloud based 3d object detection. In *Proceedings of the IEEE conference on computer vision and pattern recognition*, pages 4490–4499, 2018. [2](#)
- [36] Yi Zhuang and Haitao Zhao. Span: siampillars attention network for 3d object tracking in point clouds. *International Journal of Machine Learning and Cybernetics*, pages 1–13, 2022. [2](#)